Review Paper

Landslides (2022) 19:265–276
DOI 10.1007/s10346-021-01733-2
Received: 5 February 2021
Accepted: 25 June 2021
Published online: 26 November 2021

G. Meyrat · B. McArdell · K. Ivanova · C. Müller · P. Bartelt

A dilatant, two-layer debris flow model validated by flow density measurements at the Swiss illgraben test site

Abstract We propose a dilatant, two-layer debris flow model validated by full-scale density/saturation measurements obtained from the Swiss Illgraben test site. Like many existing models, we suppose the debris flow consists of a matrix of solid particles (rocks and boulders) that is surrounded by muddy fluid. However, we split the muddy fluid into two fractions. One part, the inter-granular fluid, is bonded to the solid matrix and fills the void space between the solid particles. The combination of solid material and inter-granular fluid forms the first layer of the debris flow. The second part of the muddy fluid is not bonded to the solid matrix and can move independently from the first layer. This free fluid forms the second layer of the debris flow. During flow the rocky particulate material is sheared which induces dilatant motions that change the location of the center-of-mass of the solid. The degree of solid shearing, as well as the amount of muddy fluid and of solid particles, leads to different flow compositions including debris flow fronts consisting of predominantly solid material, or watery debris flow tails. De-watering and the formation of muddy fluid washes can occur when the solid material deposits in the runout zone. After validating the model on two theoretical case studies, we show that the proposed model is able to capture the streamwise evolution of debris flow density in time and space for real debris flow events.

Keywords Debris flow hazards · Two-layer model · Dilatancy · Streamwise density distribution · Illgraben

Introduction

The assessment of debris flow hazard relies on both numerical simulation models [1–6] and empirical methods [7]. Most numerical approaches solve shallow-water type equations [8] and therefore can be effectively applied to predict flow heights and debris flow runout distances. Nonetheless, the application of numerical models in hazard engineering practice remains limited [9]. This is due to two salient problems. Firstly, it is difficult to quantify accurately the initial starting and entrainment masses for a specific torrent. And secondly, historical case studies are still necessary to calibrate the rheological parameters that govern debris flow motion at a specific site, and therefore possible inundation area [1, 3, 10]. Without this information, the motion of a debris flow is difficult to model because it depends strongly on the relative amounts of solid and fluid masses [11]. Typically, the front of the debris contains most of the rock material whereas the tail is more fluid like [12, 13], see Fig. 1. When the solid material stops in the runout zone, the muddy fluid de-waters from the rocky material, or is overrun by the fluid tail, creating muddy floods and channel outbreaks [14]. The varying solid/fluid composition of debris flows leads to a wide range of possible deposition behaviors, making the prediction of the hazard extent for a specific torrent highly uncertain; see [9].

Two-layer approaches that simulate both the motion of the rocky solid and muddy fluid would serve to alleviate many of these problems involved in modelling debris flows, including the specification of the initial conditions, modelling entrainment and selecting appropriate rheological parameters. This is evidenced by the recent development of several two-layer debris flow models [15–19]. To apply these two-layer debris flow models in practice we must first demonstrate that they predict the correct streamwise structure of the flow. It must be shown that the distribution of solid and fluid material from the debris flow front to tail can be accurately modelled. This is a difficult problem because it depends both on entrainment processes (the entrainment of solid material at the leading edge of the flow), detrainment (solid mass loses at the debris flow sides) as well as the momentum exchange between solid and fluid components [20]. In many ways, this problem can be considered experimental, in the sense that little data exists to substantiate/refute different model approaches that predict the evolution of flow density in the streamwise direction. Once the relative amounts of solid and fluid are known, these must be linked to follow laws that govern the bulk speed of the flow, as well as important processes such as de-watering and the eventual separation of the solid and fluid components. Again, this problem is a large part experimental, since there are few basal shear measurements of actual debris flows that would allow a testing of different modelling approaches.

In this paper we address the important problem of the distribution of solid/fluid mass in the debris flow body. Using density measurements captured at the Swiss Illgraben test site [21, 22], we model the streamwise structure of a series of debris flows. That is, we attempt to simulate the volumetric solid and fluid parts of the debris body, and therefore the flow density of the debris flow from initiation to runout. Similar to many existing approaches, we adopt a shallow-water approach because of its computational speed. Within the framework of the shallow-water approach, we must therefore divide the fluid part of the debris flow into *inter-granular* and *free* parts in order to model the separation of the solid and muddy components, and therefore processes such as de-watering and fluid flooding. The data and model results integrate a series of recent works that introduce dilatant flow mechanics [15, 23] into debris flow modelling. Although we present actual shear measurements showing how shear resistance decreases with increasing fluid content, we do not address the rheology problem here, concentrating first on capturing the streamwise variation of bulk flow density.

Fig. 1 A debris front passes a concrete check dam at the Illgraben test site on August 20, 2020. Note the blocky front and watery tail. The front appears to dam the muddy fluid flowing behind; the rocks in the tail appearing completely submerged in the muddy fluid. Saturation increases from front to tail. Photograph WSL

The rest of this paper is organized as follows: in Sections 2 and 3, we describe the basic ideas behind our two-layer model; in Section 4, we present the governing equations of debris flows (mass and momentum conservation laws), and in Section 5, we show the numerical results. The comparison to Illgraben measurements is found in Section 6. The paper is rounded off with some concluding remarks and an outlook to future work in Section 7.

Debris flow density, solid particles and muddy fluid

We consider a debris flow to be constituted of two material components: a solid component (subscript s) consisting of coarse granular sediment (e.g., boulders, cobbles, and gravel), associated with a density ρ_s, and a fluid component (subscript m) consisting of fine sediment likely to behave as suspended sediment (e.g. sand, silt, clay), hereinafter referred to as the muddy fluid content denoted by ρ_m. Although the grain-size distribution of the solid layer is likely to be important in the dynamics of debris flows [24], herein we do not consider grain size in our approach. We consider the individual solid particles to be undeformable; however, the ensemble of solid particles can be deformed and sheared, leading to different spacings between the particles. Therefore, the local bulk density of the debris flow ρ varies because it consists of a mixture of solid particles combined with different amounts of muddy fluid. For now, we will always make the assumption that the solid component is fully saturated with muddy fluid. It contains no interstitial air.

Most existing debris flow models [15–17, 19, 25] consider the solid and fluid components to be two independent phases, moving with different velocities. They assume that the first phase/layer (subscript 1) is equal to the solid component and the second phase/layer (subscript 2) to be equivalent to the muddy component. Therefore, there can be no mass exchanges between the two phases/layer. Momentum can be exchanged between the two phases by shearing and rubbing interactions between the solid particles and the fluid mud.

In our model, we make an alternative assumption: the first layer (subscript 1) consists of a mixture of solid particles *and* inter-granular muddy fluid that is bonded to the particle ensemble. The mass per unit area of this layer is denoted M_1. It consists of solid mass (M_s) and *inter-granular* fluid mass (M_b)[1]. The second layer (subscript 2) consists only of the fluid that is free to move independently of the first layer. We term this second layer the *free* fluid (subscript f) which has a mass M_f (also per unit of area), Figs. 2 and 3. These relations can be mathematically expressed as,

$$M_1 = M_s + M_b = \rho_s h_s + \rho_m h_b = \rho_{sb} \underbrace{(h_s + h_b)}_{h_{sb}} \tag{1}$$

$$= \rho_s \underbrace{(h_s + \frac{\rho_m}{\rho_s} h_b)}_{h_1} \tag{2}$$

$$M_2 = M_f = \rho_m h_f. \tag{3}$$

The heights h_s and h_b represent the height of the solid and inter-granular fluid components; they can likewise be considered as volumetric parts of the debris flow mass. Be aware that even if h_{sb} and $h_2 = h_f$ represent real heights of the first and second layers, this is not the case for h_s and h_b which represent the volumetric concentrations of solid and inter-granular fluid in the first layer, respectively. The same remark holds for h_1 which does not have any physical meaning but is added to simplify the shallow water equations, Section 4. The total mass of the debris flow M is the sum of the mass of layer 1 (solid particles and inter-granular fluid) and mass of layer 2 (free fluid),

[1] The index 'b' stand for 'bonded'.

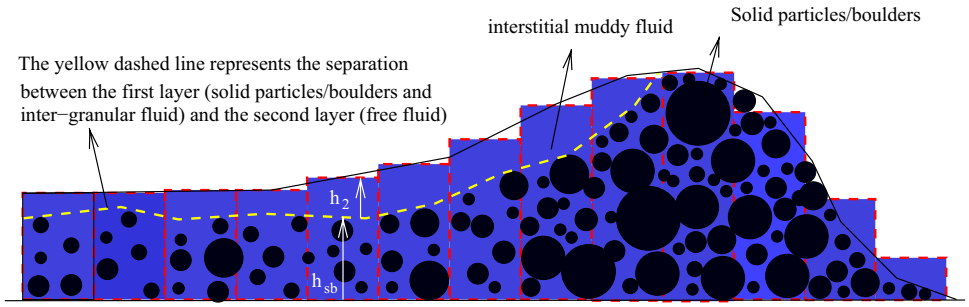

Fig. 2 The debris flow is divided into a serie of volumes *V*. The flowing material is separate into two layers. The first layer is composed by all the solid mass (particles and boulders) and inter-granular fluid (h_{sb}), while the second layer is only composed by free fluid, (h_f), flowing on top of the first one. The density of the first layer can vary from dense flowing configurations (front of the debris flow) to wet flowing configurations (tail of the debris flow) under dilatancy, see Section 3 and Fig. 3

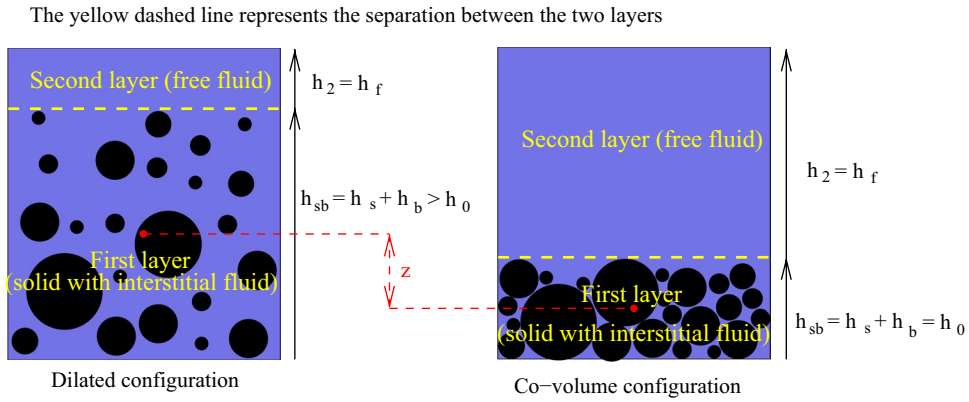

Fig. 3 Sketch of two different debris flow configurations, possessing the same amount of solid and fluid mass. The left one is a dilated configuration, happening during flowing, while the right one is the reference configuration, called the co-volume configuration, typically when the flow is at rest. The different heights we have defined in Sections 2 and 3 are depicted here. The red dots show the center of mass of the corresponding configuration. The parameters *z*, introduced in Eq. 6, is the difference between the centers of mass of the dilated and co-volume configuration

$$M = M_1 + M_2 = M_s + \underbrace{M_b + M_f}_{M_m} = \rho_s h_s + \rho_m \underbrace{(h_b + h_f)}_{h_m} \tag{4}$$

where h_m defines the total amount of fluid in the flow. In order to completely define our mass in a given volume, the last step is to differentiate the inter-granular and the free fluid. This is accomplished by assuming that the separation between the inter-granular and the free fluid is given by the location of the highest solid particle. We suppose that the solid content is homogeneously distributed in the first layer. Therefore, the center of mass of the solid is $\frac{h_{sb}}{2}$. Moreover, all the fluid which fills the void space is considered as bonded (it forms the inter-granular fluid component) and all the remaining fluid, is considered as free (see Figs. 2 and 3). All the fluid which flows above the first layer is considered free, and subsequently it can escape the matrix of solid particles, allowing the debris flow to de-water. Thus, fluid can escape from the solid part of the flow.

Finally, we denote the velocity of layer 1 as $\mathbf{v}_1$[2]; the velocity of the second layer is $\mathbf{v}_2$. The velocity is a vector quantity as we consider velocity to be in two plane-parallel directions given by the digital terrain model.

Dilatancy in the solid boulder matrix

The basic idea behind our model is to describe the debris flow as a dilating mixture of solid particles (boulders, rocks) and muddy fluid. Because of shearing interactions between the individual particles and the ground, the solid matrix dilates; that is, the spacing between the particles can increase or decrease, changing the overall volume of the first layer, [26]. More precisely, in our model, dilatancy will be responsible of fluid mass exchanges between the two layers. These mass exchanges will change the flow composition and allow us to have a varying density profile inside the flow. Indeed, without dilatancy, our model would be closer to two independent one-layer model than a real two-layer model with interactions. Therefore, the density evolution in our model is the consequence of dilatancy.

We define three variables associated with the solid mass, h_s, h_0 and h_{sb}. The height h_s is the volume of the solid particles in the flow,

[2] We assume zero slip between the granules and the inter-granular fluid.

h_0 represents the reference height of the non-dilated mass[3], whereas h_{sb} represents the dilated height of the solid mass, Section 2 (see Fig. 3). We refer to h_0 as the *co-volume*, in an analogy to Van der Waals work on non-ideal gasses with large molecules and cohesion [27]. Note that, even if the solid mass is conserved, the first layer density can vary, according to Eq. 1, if the inter-granular fluid concentration evolves :

$$\rho_{sb} = \frac{\rho_s h_s + \rho_m h_b}{h_s + h_b} \tag{5}$$

The potential energy D (per unit area) associated with the dilatation of solid material is

$$D = \underbrace{\left[\rho_s - \rho_m\right] h_s}_{\text{buoyant mass}}\, g\, \underbrace{\frac{1}{2}\left[h_{sb} - h_0\right]}_{z}. \tag{6}$$

where z is the distance between the center of mass of the dilated configuration and the co-volume one, Fig. 3. Because the configuration of the particles in the dilated volume defines the potential energy D, we sometimes refer to the energy D as the *configurational energy* of the debris flow [28–30]. Importantly, we are making the following physical assumption: the potential energy is associated with the *buoyant weight* of the solid particles immersed in the inter-granular fluid. Any change in z implies a change in the potential energy, $\Delta D \propto \Delta z$.

For a debris flow, changes in void space are always associated with movement of the interstitial muddy fluid. When the void space between particles increases, fluid will fill the space between particles, or conversely, when the void space decreases, fluid will be squeezed out. Fluid mass that fills the void space will eventually move at the same speed as the particles and therefore becomes inter-granular, whereas fluid that is squeezed out becomes free to move independent of the particulate mass. This implies there is a mass exchange between the inter-granular and the free fluid components, that depends on the void space of the solid mass. If the flow is dilating, typically just after the release, free fluid is transformed into inter-granular fluid. Inversely, if the solid void space is decreasing (e.g. in the run-out area) the rate of fluid exchange changes, and inter-granular fluid becomes free (de-watering). To model this effect, we let $\dot{q}$ denote the rate of the fluid mass exchanges. It can be calculated directly from any change in the distance between the center-of-masses of the reference and dilated configurations Δz,

$$\dot{q}\Delta t = \Delta z. \tag{7}$$

In this paper the configurational energy D is governed by a simple production (parameter α) and decay (parameter β) term, similarly to what has been used for snow avalanches, see [26]:

$$\frac{\partial D}{\partial t} + \vec{\nabla} \cdot (D\mathbf{v}_1) = \alpha \dot{W}_f - \beta D. \tag{8}$$

The quantity W_f represents the shear work. That is, the change in the energy of configuration D (dilatation) is directly related to the shear work, in accordance with Reynolds [31]. The parameter α defines the fraction of the shear work that produces a dilatation, whereas the parameter β defines how quickly the dilatation collapses in the absence of shear, due to energy dissipation caused by shearing between particles. The balance between the production of D and its decay essentially defines the degree of saturation in the debris flow, as this defines the amount of void space (inter-granular water) in the moving solid. As we will show in the final section, the parameters α and β can be determined from experimental measurements such as the ones in Illgraben.

An important fact is that mass exchanges between the inter-granular and free fluid components are also associated with a transfer of momentum ($\vec{P}$) between the two debris layers.

Model equations

Depth-averaged mass conservation equations can be written for the three material components h_b (inter-granular fluid), h_1 (first layer) and h_2=h_f (free fluid),

$$\frac{\partial h_b}{\partial t} + \vec{\nabla} \cdot (h_b \vec{v}_1) = \dot{q} \qquad \text{inter-granular fluid} \tag{9}$$

$$\frac{\partial h_1}{\partial t} + \vec{\nabla} \cdot (h_1 \vec{v}_1) = \frac{\rho_m}{\rho_s} \dot{q} \qquad \text{first layer} \tag{10}$$

$$\frac{\partial h_2}{\partial t} + \vec{\nabla} \cdot (h_2 \vec{v}_2) = -\dot{q} \qquad \text{free fluid} \tag{11}$$

where $\vec{\nabla}$ is the divergence operator in Cartesian coordinates. The right-hand side of the inter-granular fluid and free fluid equations contains the term $\dot{q}$, Eq. 7, which is the mass exchange rate between the inter-granular and free fluid because of dilatant actions in the solid matrix. In Eq. 10, as well as in Eq. 12, we include the density as the left hand side contains the density ρ_s, Eq. 2, while the right hand side contains the density of the muddy fluid. Here we assume no entrainment of solid material from the mountain torrent. Note that in Eq. 10, as well as in Eq. 12, we use h_1 instead of h_{sb}. Indeed, h_1 has a constant density, which allows us to simplify the equations. In this form, the equations are mass conservative. Note also that it is possible to find the equation for the boulders/solid content of the flow combining Eq. 9 and 10 together with Eq. 2.

We have in total four momentum conservation equations, viz. two equations for each of the two layers. If $b := b(x, y)$ denotes the bottom topography, they can be written in vectorial form as [32, 33]:

$$\partial_t(h_1\vec{v}_1) + \vec{\nabla} \cdot \left(h_1\vec{v}_1 \otimes \vec{v}_1 + \frac{gh_1^2}{2} I\right) + gh_1\vec{\nabla}\left(b + \frac{\rho_m}{\rho_s} h_2\right) = -\vec{S}_1 + \frac{\rho_m}{\rho_s}\dot{\vec{P}} \tag{12}$$

$$\partial_t(h_2\vec{v}_2) + \vec{\nabla} \cdot \left(h_2\vec{v}_2 \otimes \vec{v}_2 + \frac{gh_2^2}{2} I\right) + gh_2\vec{\nabla}\left(b + h_1\right) = -\vec{S}_2 - \dot{\vec{P}} \tag{13}$$

The first, resp. second, equation represents the first, resp. second, layer. The symbol $\otimes$ denotes the tensor product and I is the two-dimensional unity matrix. The left side is the total variation of the momentum with respect to time, including the effect of gravitation and the influence on one phase to the other, [32, 33]. The right side represents the change in momentum due to external forces (excluding gravitation). $\vec{S}_i$ is the shearing forces acting on the ith layer. As

[3] It is different from h_s, because we consider that, even in the non-dilated configuration, the void space is not zero.

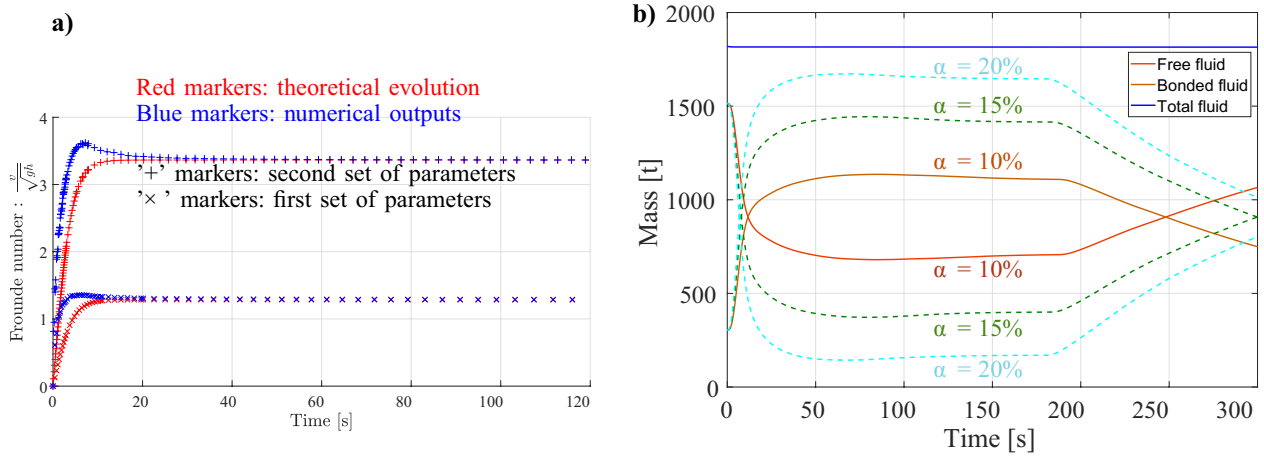

Fig. 4 **a**) Results of two simulation checks. For a flow on a flat slope governed by Voellmy-type friction parameters, the Froude number is constant at steady state. **b**) The total fluid mass composing the flow is plotted as a function of the time. The dark orange line is the inter-granular fluid, the light orange line is the free fluid; the blue line is the total amount of fluid, i.e., the sum of the two previous ones, for $\alpha = 10\%$. The dashed line represent the inter-granular (upper curves)-free(lower curves) fluid evolution for two different values of *alpha*, i.e. $\alpha = 15\%$ (green dashed lines) and $\alpha = 20\%$ (cyan dashed lines). Total fluid is conserved as slope changes cause unsteady motions

we are using the Voellmy–Salm model [34], the shearing forces (per unit of area A) can be expressed as:

$$\vec{S}_i = \left(\mu_i g_z h_i + \frac{g||v_i||^2}{\xi_i}\right)\hat{e}_i \tag{14}$$

where $\hat{e}_i$ is the unit vector along the flowing direction : $\hat{e}_i = (\frac{v_{i,x}}{||v_i||}, \frac{v_{i,y}}{||v_i||})^T$. The gravity component g_z is the slope-perpendicular acceleration due to gravity, $g_z = g\sin(\theta)$ where θ is the slope angle of the corresponding cell. We emphasize that we neglect the shearing between the two layers. Indeed, we can consider the shearing processes acting at the interface between the two layers as a Coulomb type friction. However, we use a value of the fluid Coulomb coefficient close to zero ($\mu_2 \approx 0.01$). Therefore, the shearing between the two layers can be assumed negligible.

Finally, $\dot{P}$ is the rate of momentum exchange associated with the mass exchange. Because Eq. 12 is defined per unit of ρ_s, while Eq. 13 is defined per unit of ρ_m. Together, these terms invoke Newtons' third law of action and reaction between the layers. The momentum exchange rate can be expressed as:

$$\dot{\mathbf{P}} = \begin{cases} \dot{q}\vec{v}_2 & \text{if the first layer is dilating} \quad \dot{h}_1 > 0 \\ \dot{q}\vec{v}_1 & \text{if the first layer is collapsing} \quad \dot{h}_1 < 0 \end{cases} \tag{15}$$

Numerical validation

Various numerical schemes for depth-averaged shallow-water type equations can be applied to solve numerically this system of equations [8, 35, 36]. We numerically solve equations Eqs. 8 -13 using finite volume schemes within the RAMMS avalanche software [37]. The equations are solved in two steps. First, we solve the hyperbolic part of the equations, i.e. without the source term (right-hand side) using a second order ENO scheme. The second step is to integrate the source terms using a second order Runge-Kutta method.

To check the mathematical consistency of the model (Eqs. 6 and 8 to 13), we performed two numerical tests. The first test is designed to test the stability of the three-component momentum equations (solid, free and inter-granular fluid), while the second test is designed to check the mass conservation between the inter-granular and free fluid contents during dilatative changes in the solid boulder/rock matrix.

The first test is based on the idea that for a steady flow, the dimensionless Froude number is constant, defined only by the Voellmy-type friction parameters μ and ξ in relation to the slope angle θ. This condition must hold for the two-component flow (inter-granular fluid/solid material) even if the solid material is undergoing shearing and dilatative changes. The derivation of this fact is contained in a short Appendix. We therefore performed block release simulations on a flat plane with a uniform slope angle, Fig. 4a. The plane connects to a flat runout area. In order to prove the existence of steady state, our interest is directed toward the slope above the runout plane. Obviously in real-terrain conditions, the flow would generally not reach a pure steady state configuration.

The convergence of the numerical simulations to the theoretical results is depicted in Fig. 4a (input parameters are summarized in Table 1). Here, the Froude number is plotted as a function of the simulation time t. The red curves represent the theoretical Froude numbers evolution for a sliding rigid block (see Appendix) for two

Table 1 Summary of the free parameters governing the Froude number value

Simulation	μ []	ξ [m/s^2]	θ [°]	Froude Number
1 ('x')	0.1	100	15	1.29
2 ('+')	0.15	300	30	3.36

different sets of friction values (Table 1, markers 'x' and '+'), while the blue markers are the numerical outputs. The mass of the block used in the theoretical computation is equivalent to the initial mass of the release block used in the numerical simulations. This plot reveals an important feature of model; namely, that in steady state, there are no dilatative changes in the solid boulder/rock matrix. The flow density is constant in steady state, and therefore, there is no changes in the amounts of free and inter-granular fluid components. Indeed, momentum exchanges would result in a deviation in the Froude number convergence. Therefore, a constant Froude number, which coincides with the mathematically computed value, means that no momentum exchanges are occurring, which is the proof that the flow has attained a constant density[4]. Changes in slope angle encountered in real torrents therefore always produce changes in the debris flow density and streamwise structure.

Note that in the mathematical derivation of the Froude number value, Appendix, we do not consider the influence of one phase on each other. However, this effect is taken into account when we performed the numerical simulations. The fact that the numerical output converges to the theoretical value shows that these effects are negligible. Therefore, the mathematical derivation can be considered as valid even for a dilatant two-layer model with phase interactions.

The second consistency check demonstrates that when the debris flow is outside steady state, and there are changes in the streamwise structure and dilatant actions in the boulder/rock component, the mass of free and inter-granular fluid (total fluid) are always conserved. Therefore, for model consistency, we have to check that the entire amount of fluid contained in the flow is conserved with time. The simulations are again perform on an ideal, flat plane with a constant 30°slope. This time, however, we are interested when the flow leaves the slope and enters the runout zone; that is, when the flow is no longer in steady state as in the previous case. We have plotted the mass of the different fluid flow components as a function of the time for three values of α : 10%, 15% and 20%, Fig. 4b. The orange and red curves represent the free and inter-granular fluid for $\alpha = 10\%$, while the blue lines are the total fluid composing the flow (sum of the two previous curves). the green and cyan dashed lines are the evolution of free(lower curves) and inter-granular (upper curves) fluid, for $\alpha = 15\%$ and $\alpha = 20\%$. This result demonstrates that fluid mass is conserved during unsteady motions in uneven terrain. Moreover, we can check that the mass exchanges (and therefore the debris flow saturation), increase with α, which is the consistent numerical behavior.

Comparison to illgraben measurements

The Illgraben debris flow test site (Fig. 5) is located near Leuk, Canton Valais, Switzerland [11, 21, 22]. Since 2005, the Illgraben torrent has been instrumented with a rectangular force plate (area A=4m^2) that measures shear (S) and normal (N) stresses at the base of a passing debris flow. A laser sensor located above the plate measures the total debris flow height h as the flow passes over the plate. The force plate is located at the end of a 2.5-km-long torrent (in orange on Fig. 5) that has an average slope of 5°. The torrent is fed

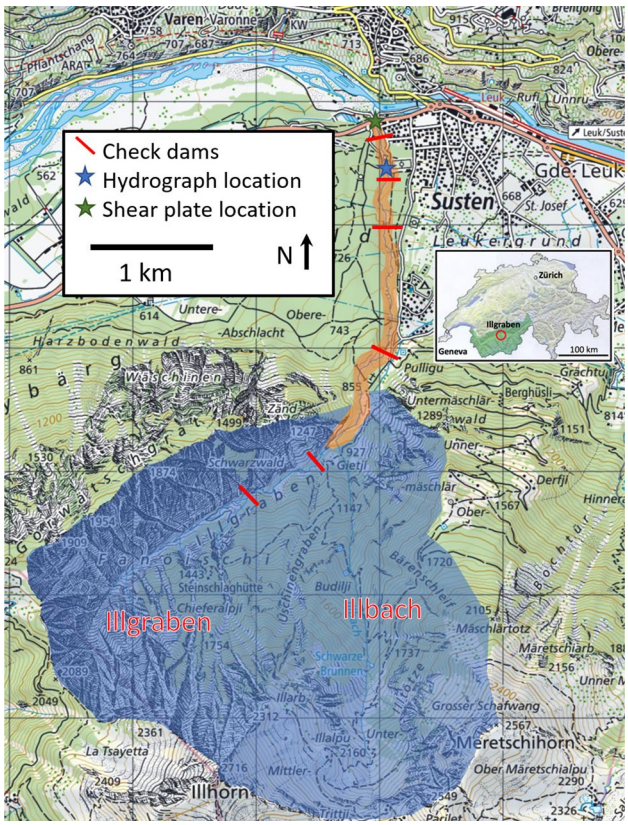

Fig. 5 Map of the Illgraben test site. The catchment zone is given by the blue polygon, while the channel is drawn in orange. The check dams are also shown (red line). The blue star represents the starting point of the hydrogaph, used for the numerical simulation, and the green star is the location of the shear plate. The original map can be found in [11]

by a large (9.5km^2), steep catchment zone (in blue on Fig. 5), which supplies the measuring channel with debris flows of various sediment/fluid compositions. In this paper we consider four specific debris events, see Table 2. All four events can be considered single surges, with well-defined front-tail structure. The debris flow fronts contained boulders and rocks, leading to large measured normal stresses $N \approx$ 20kPa - 25kPa (Fig. 6a, b, c, d). The debris flow fronts were followed by fluid tails containing much less solid mass, reducing the measured normal stresses.

From the measurement data it is possible to estimate the streamwise bulk density ρ of the flow, and therefore the time variation of the solid and fluid components as debris flow passes over the plate. Keeping the same notation as in Section 2, we can write the two following equations:

$$h = h_s + h_m \tag{16}$$

$$M = \frac{N}{g_z} = (\rho_s h_s + \rho_m h_m)A = \rho h A. \tag{17}$$

In these equations, M is the total mass running over the plate which has the mean bulk density ρ. As the basal area A is constant we can represent the volumetric components of the solid/fluid as a

[4] A constant density does not mean that the steamwise density distribution is uniform.

Table 2 Main characteristics of the simulated debris flows

Event	Description	≈ Max flow height	≈ Time event	≈ Front velocity
(a) 02.08.2005	Event with a high density: rocky event	1.1 m	20 min	no data
(b) 28.07.2006	Unconventional event the tail becomes again less saturated	1.5 m	55 min	2 m/s
(c) 31.08.2008	Rocky front and very fluid tail, large saturation difference between the front and the tail	1.4 m	25 min	1.9 m/s
(d) 29.07.2013	extremely fluid event	1 m	50 min	1.9 m/s

corresponding height. Gravity g_z is the slope-perpendicular gravity component. With these equations, we can equivalently write,

$$\rho = \frac{\rho_s h_s + \rho_m h_m}{h_s + h_m} \tag{18}$$

$$\begin{aligned} h_s &= h\left[\frac{\rho - \rho_m}{\rho_s - \rho_m}\right] \\ h_m &= h\left[\frac{\rho_s - \rho}{\rho_s - \rho_m}\right]. \end{aligned} \tag{19}$$

Therefore, thanks to this experimental setup, we can extract from the measurements the streamwise evolution of the bulk density, Eq. 18. (Equivalently it is possible to calculate the volumetric fluid concentration $\frac{h_f}{h}$). In the four events studied, the variation of the density with respect to time is highly different from one event to the others (Fig. 6a, b, c, d). However, the variation of the density with the normal stress exhibits a similar behavior for each of the measured events (Fig. 7a, b, c, d). The color is an additional time information. The blue markers represent the front of the flow and time is evolving as we approach the yellow color. From this time information, we can check that the flow density is higher in the front (blue) than in the tail (yellow). As a consequence of the uniformity in the density-normal stress space, we compare the density behavior with respect to the normal stress, rather than the time variation of the flow composition itself.

In Fig. 6a, b, c, and d, the debris flow height (colored curves) and the density (black curves) is plotted as a function of time for the four different events. Colour should help to guide the reader over the duration of the event. However, be aware that the color is more an indication than a real temporal data. Indeed, for both subgraphics, the two curves (Illgraben data and numerical outputs)

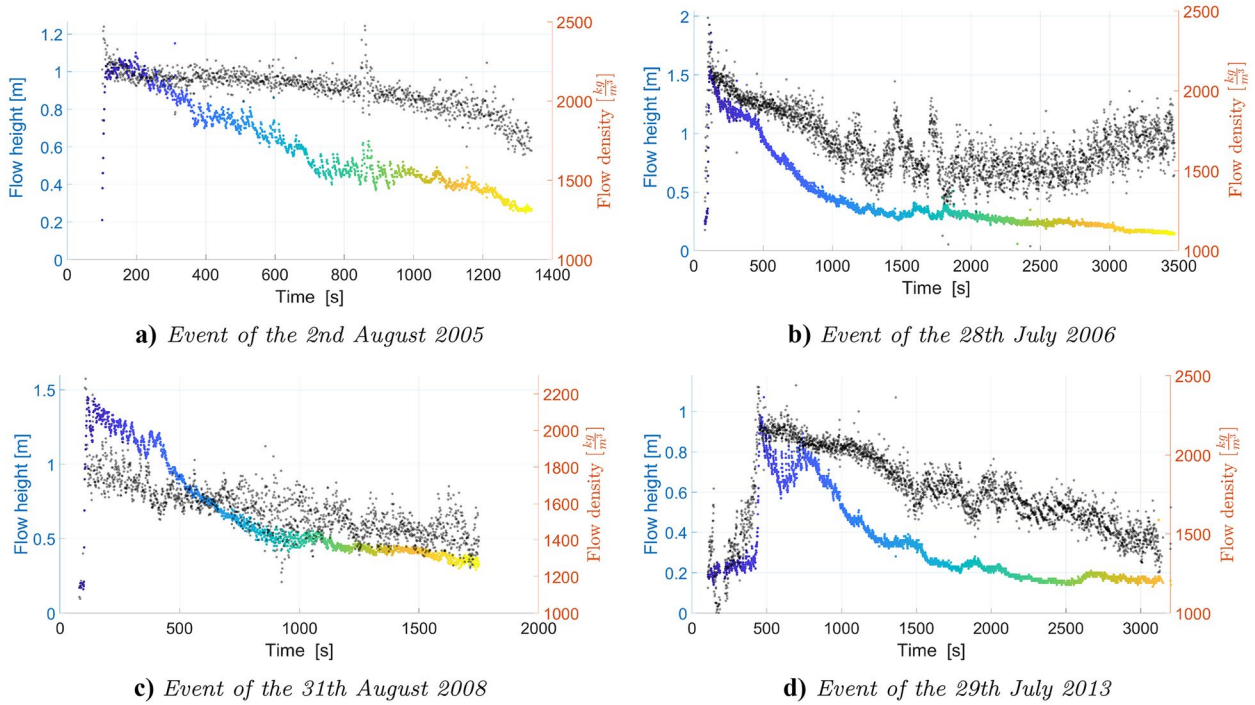

Fig. 6 Data of the Illgraben data measurements. The colored markers plot the flow height behavior, whereas the black markers plot the density evolution. Both markers are plotted with respect to time. The color is an additional temporal information, the blue represents the front and the yellow the tail

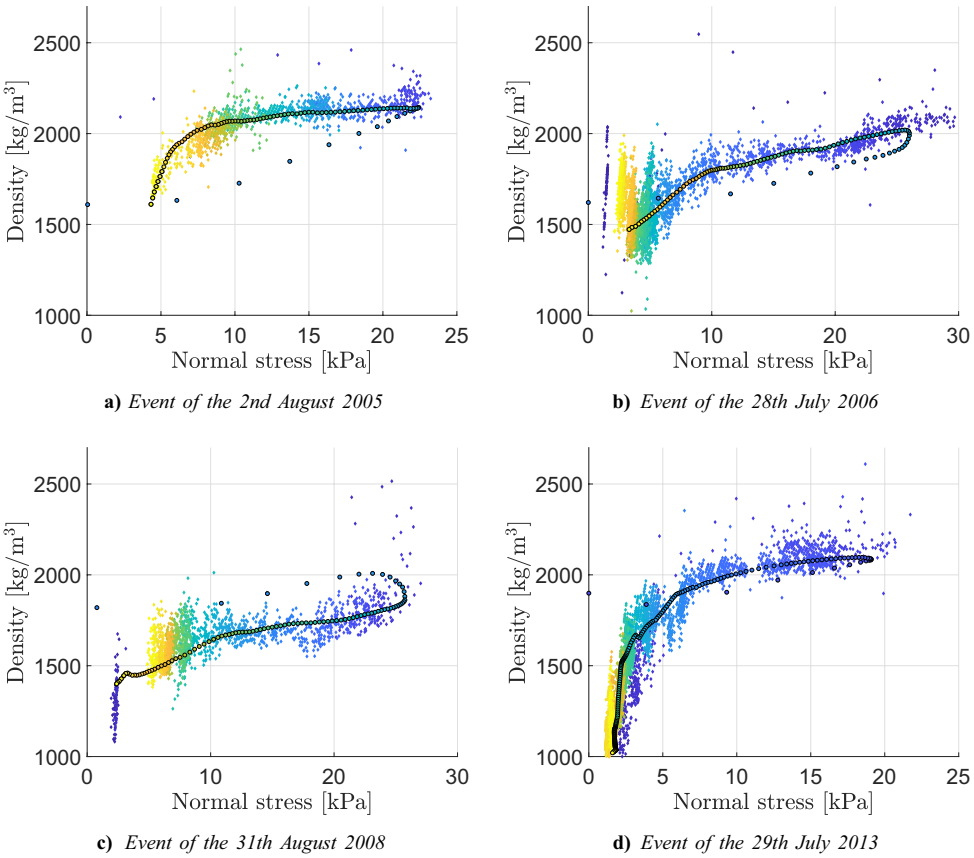

a) *Event of the 2nd August 2005*

b) *Event of the 28th July 2006*

c) *Event of the 31th August 2008*

d) *Event of the 29th July 2013*

Fig. 7 Comparison between Illgraben data and numerical simulations results. Bulk density ρ as a function of normal stress N. The colored dots are the experimental data while the black edge dots are the numerical outputs. The color is an additional temporal information, the blue represents the front and the yellow the tail

do not have the same duration. Therefore, the yellow markers, by instance, represent in both (Illgraben and numerical simulation) case the end of the flow, but are associated with different times.

To validate our model, we have selected four events at the Illgraben site: the 2nd of August 2005, the 28th July 2006, the 31st August 2008 and the 29th July 2013. We use a hydrograph for the release method [38]. In order to compare the numerical prediction with the experimental results, we have selected four cells (a square of 2 by 2 cells), corresponding to the shear place location. For comparison we used the average of different variable of the debris flow on these cells.

The comparison between experimental and numerical results is shown in Fig. 7a, b, c, d, which plots the first layer density as a function of the first layer normal stress. The colored dots are the experimental data while the black edge symbols, filled with color, are the numerical outputs. These results suggest that the dilatant, two-component model is able to reproduce the streamwise density structure of several debris flows observed at the Illgraben test site. The numerical results not only predict the correct dependency between density and normal stress, but also the correct time dependency. Although this is a positive result, it must be emphasized that the model is not able to differentiate between the inter-granular and free fluid components and therefore the exact degree of solid dilatation. This is largely due to the fact that the Illgraben data, although extensive, does not provide a means to separate the inter-granular and fluid parts of the interstitial muddy fluid. We are able only to measure the sum of the muddy fluid passing the normal plate over time. This leads to an important observation: as we cannot distinguish the interstitial and free fluid from the Illgraben measurements, we can choose to match the experimental data either with the first layer density or with the entire debris flow density. We have chosen the former case for the following reason. Our final goal is to compute the flow rheology as a function of the flow composition. However, in our model, the rheology of the first layer only will change, because the second layer is completely composed by fluid. Therefore, it is relevant to match the data with the first layer only, as this will determine in large part the rheology of the flow[5]. Moreover, we can also choose to initialize the flow in a already dilated configuration, in which case all the fluid is assigned to belong to the first layer and there is no free fluid as long as the solid matrix does not start to collapse. However, we did not use this way to initialize the flow for consistency reasons. Indeed, we wanted to show that we were able to catch the right density profile even when we initialize the flow in the co-volume configuration, to demonstrate the applicability of the dilatancy approach.

As a last results, we show on Fig. 8, the time-spatial evolution of the three flow contents, that is to say: the solid matrix, the interstitial fluid, and the free fluid. One can see an important aspect of the model. During flow, the amount of free fluid is small with respect to the first layer, which is the sum of the two left plots.

[5] We can also possible to match the Illgraben measurements with the entire flow data.

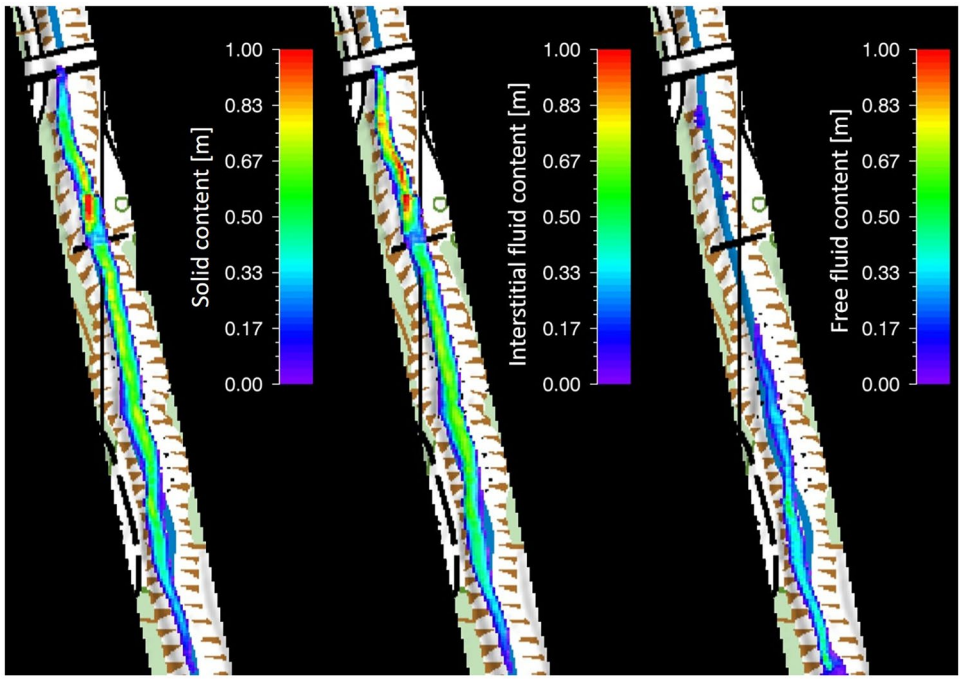

Fig. 8 Three pictures of the simulations performed to match the 2013 event. From left to right: the solid height, the interstitial fluid height and the free fluid height. The picture is taken when the first layer reaches the shear plate. We can see here an important point of the model: during flowing, a large part of the fluid belongs to the first layer and there is only a small amount of free fluid left

Discussion and conclusions

Measurements of *S*/*N* ratios of debris flow reveal a strong decrease in friction with increasing volumetric fluid content (Fig. 9a, b, c, d). This statement can, of course, be alternatively stated: *S*/*N* ratios increase with increasing solid content. However, the experimental data reveals an important second point: the solid/fluid content distribution varies in the streamwise direction. Often, the debris flow front contains less fluid than the tail, indicative of higher friction, or bulking, at the leading edge of the flow (Fig. 6a, b, c, d). The solid mass will have a tendency to stop sooner, in comparison with the fluid concentrated tails, causing a wide array of different stopping possibilities in runout zones. Stopped solid concentrations can de-water, or be overflown by their muddy tails. Torrents can be blocked and dammed, leading to channel outbreaks and muddy flows that inundate large areas.

The first step to model accurately the mobility of a debris flow is the ability to predict the variation of volumetric fluid/solid components—essentially the streamwise variation of the bulk density from the head to the tail of the flow. This task cannot be achieved within the framework of simple one-layer models and is the purpose of this paper.

The approach adopted in this paper is to divide the fluid content into two parts—the inter-granular part (that moves with the speed of the solid matrix) and the free fluid (which moves independently from the solid). We assume that all fluid that can be contained in the void space of the solid is inter-granular. The problem here is that the void space is continuously changing because of the continuous interactions between the rocks and boulders themselves and the ground. Shearing changes the volume of the solid matrix and thus the relative amounts of inter-granular and free fluid. Importantly, the solid concentration moderates the speed of the overall flow, causing the fluid to move at a slower speed, backing up the fluid into the tail of the debris flow. With this approach, it was possible to simulate the density variation (i.e., the volumetric fractions of solid/fluid) in the streamwise direction.

The model imposes two physical constraints:

1. *In steady state, there is no variation in the solid configuration, and therefore the density is constant*. Volumetric dilatation in the solid matrix are governed by the balance between the shear work rate (production) and collapse of the volume in the surrounding fluid (decay). In steady state the work done by shearing is constant and equal to the collapse rate, leading to a constant solid volume and therefore a constant void ratio. In this case there can be no exchange between the inter-granular and free fluid fractions which remain constant. This leads to constant Froude numbers in the steady state, and, because no mass can be exchanged, in turn to no momentum exchange between the two components. On steep slopes, the production term dominates leading to more dilated flows with suspended particles. In the runout zone, the flows collapse, the particles return to the basal layer and the void space disappears. The debris flows de-waters.
2. *Mass exchanges imply momentum exchanges*. In existing debris flow models [15–17, 19], momentum exchanges must be devised to regulate the speed of the two phases/layers solid/fluid models. By transferring mass between the inter-granular fluid locked in the solid matrix and the free fluid, we also transfer momentum. The transfer of momentum is regulated by the void space (dilatation) in the solid boulder/rock matrix of the flow. As we have demonstrated in the numerical examples, these momentum exchanges will only occur when the flow is in a non-steady state. For example, when the flow is undergoing sharp slope changes such as when entering the runout zone. Of importance, is the fact that the transfer of mass and momentum between the solid/inter-granular fluid (layer 1) and free fluid (layer 2) layers regulates both the speed and the density of the debris flow.

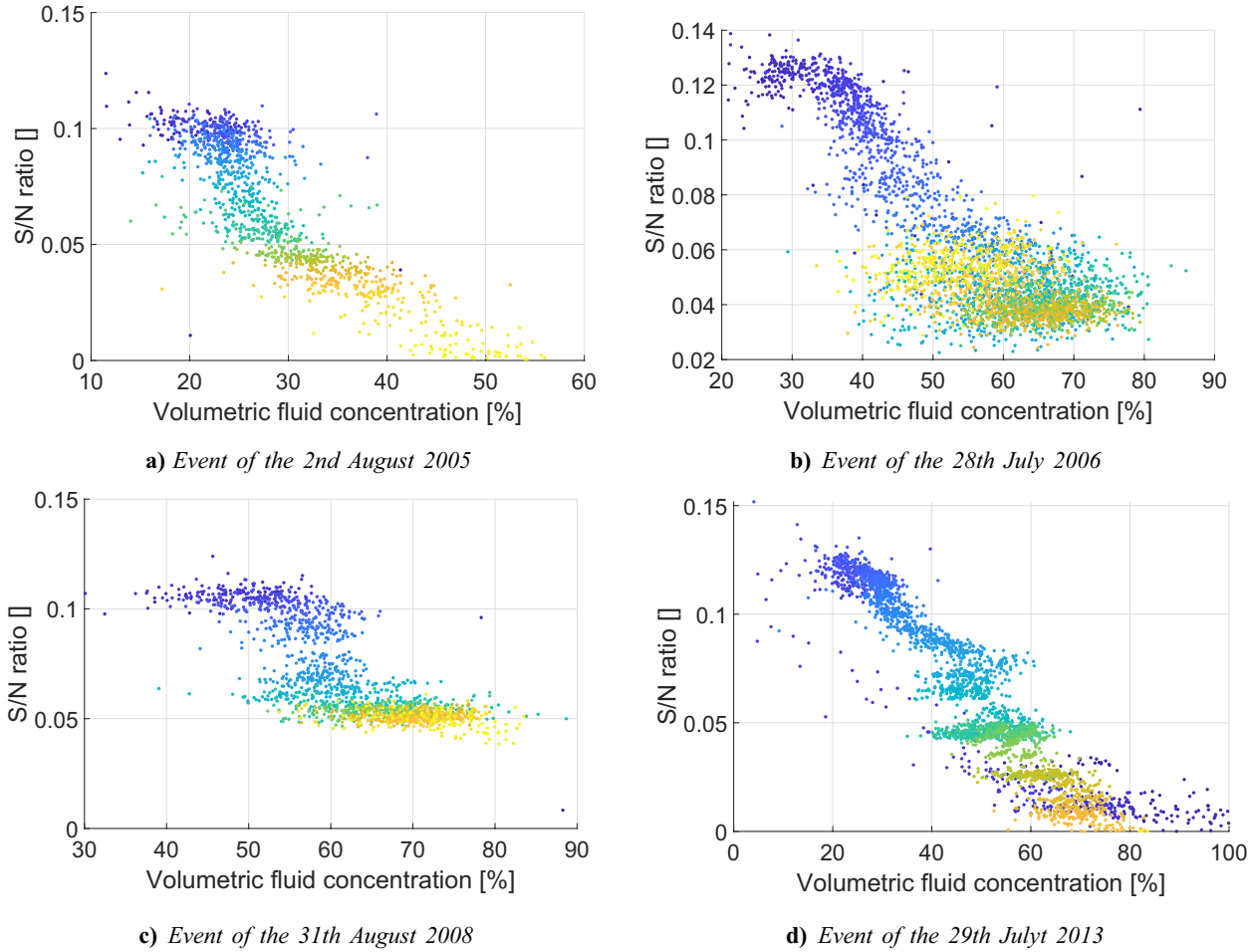

Fig. 9 Experimentally measured *S/N* ratio as a function of the measured saturation. Each dot represents an experimental measurement. The color is an additional temporal information, the blue represents the debris flow front and the yellow the tail

In our debris flow model formulation, the free fluid has two main roles. First, it surrounds the solid matrix and therefore facilitates the buoyant dispersion of the solid mass. It effectively allows dilatancy and therefore streamwise density variations. Secondly, when the solid matrix stops, the solid particles deposit out of the fluid content. It then becomes possible to simulate phase separation (dewatering) between the solid and free fluid.

Alternatively, when the debris flow mixture is still flowing, a significant proportion of the fluid is flowing at the same speed as the solid in the inter-granular void space. The amount of the free fluid layer is small comparing to the first layer, Fig. 8, in some cases nonexistent. Another important practical point is that we can initiate the flow in an already dilated configuration by using an hydrograph. Therefore, we start the debris flow as a single layer flow, assigning all fluid to be inter-granular. It means that in this case, the two-layer model reduces to a one-layer model, which implies a reduction in computational time, while keeping the possibility to have a density profile. Only in the runout zone, when the solid matrix deposits, will the inter-granular fluid become free.

To summarize, our model is able to predict the complexities of two-layer behavior (streamwise density distribution, phase separation), while solving, for a large part of the simulation time, a system of one layer equations. This offers the possibility to reduce calculation time, which is an crucial aspect in practical engineering applications. With regard to the flow rheology, we note that the experimental decrease in *S/N* (Fig. 9a, b, c, d) appears almost linear with volumetric fluid content, providing strong evidence of effective stress like

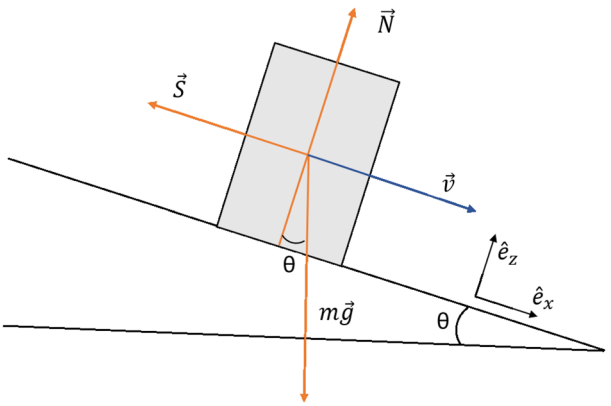

Fig. 10 Block sliding on a flat plan with constant slope angle θ

concepts which reduce the shear stress linearly with increasing fluid pressure. A first step to develop and test different two-layer rheological models is first to capture the streamwise density variation of the flow. Although our major goal was to develop a model for practical applications, because we can define variable amounts of solid and muddy fluid, the model might help also to understand how debris flow mobility will be affected in a changing climate, where we expect changing geomorphological and precipitation conditions.

Appendix

Appendix A: Analysis of a sliding block along an inclined plan with a Vollemy– type shearing model

In this section, we study the mathematical solution of a sliding rigid block along an inclined plan with a constant slope angle θ. The shearing force will be given by the Vollemy– type model. it means :

$$\mathbf{S} = \mu N \hat{e}_{\mathbf{v}} + \frac{\rho g A}{\xi} v^2 \hat{e}_{\mathbf{v}} = \left(\mu N + \frac{\rho g A v^2}{\xi} \right) \hat{e}_x \tag{20}$$

where A is the basal area, $\mathbf{v}$ is the center of mass velocity, always parallel to the slope direction $\hat{e}_x$ (we suppose than either the ground and the block are unalterable). If we use the second law of Newton and we decompose the forces along $\hat{e}_x$ and $\hat{e}_z$, slope perpendicular direction (see Fig. 10) , it gives:

$$\text{along} \quad \hat{e}_x \quad \rightarrow \quad mg \sin(\theta) - \frac{\rho g A v^2}{\xi} - \mu N = ma = m\dot{v} \tag{21}$$

$$\text{along} \quad \hat{e}_z \quad \rightarrow \quad -mg \cos(\theta) + N = 0 \tag{22}$$

Combining these two equations, we find a first order differential equation:

$$mg \sin(\theta) - \frac{\rho g A}{\xi} v^2 - \mu mg \cos(\theta) = m\dot{v} \tag{23}$$

We can solve it with respect to v. After integration, with the initial condition $v(t = 0) = 0$ we obtain:

$$v(t) = \frac{\Gamma}{\sqrt{\nu}} \tanh\left(\frac{\Gamma \sqrt{\nu}}{m} t \right) \tag{24}$$

with $\Gamma^2 = mg(\sin(\theta) - \mu \cos(\theta))$ and $\nu = \frac{\rho g A}{\xi}$. Therefore, for time long enough ($\lim_{t \to \infty}$), the block reaches a steady state, given by the steady value:

$$Fr = \lim_{t \to +\infty} \frac{v(t)}{\sqrt{gh(t)}} = \sqrt{\frac{\xi(\sin(\theta) - \mu \cos(\theta))}{g}} \left[\underbrace{\lim_{t \to +\infty} \tanh\left(\frac{\Gamma \sqrt{\nu}}{m} t \right)}_{=1} \right] \tag{25}$$

$$= \sqrt{\frac{\xi(\sin(\theta) - \mu \cos(\theta))}{g}} \tag{26}$$

which is the well known Froude number. It means that, once the entire flow (each cell) reaches a steady state, the value of the Froude number should converge to a constant and uniform value which depends only on the slope angle and the two friction parameters of the Voellmy-Salm model. We can note, that even if the mathematical derivation remains valid for every density of the block, momentum exchanges between the layers would not conserve the Froude number convergence. Therefore, to have a correspondence between the numerical output and the mathematical analysis, momentum exchanges have to be zero, which reflect the fact that we have a constant density (not uniform!!).

Acknowledgements

The authors acknowledge the support of the CCAMM (Climate Change and Alpine Mass Movements) research initiative of the Swiss Federal Institute for Forest, Snow and Landscape Research. We are especially thankful for the support of Dr. A. Bast program coordinator.

Funding

Open Access funding provided by Lib4RI – Library for the Research Institutes within the ETH Domain: Eawag, Empa, PSI & WSL.

References

1. Denlinger RP, Iverson RM (2001) Flow of variably fluidized granular masses across three-dimensional terrain: 2. numerical predictions and experimental tests. J Geophys Res: Solid Earth 106(B1):553–566
2. Hungr O (1995) A model for the runout analysis of rapid flow slides, debris flows and avalanches. Can Geotech J 32:610–623
3. Iverson RM, Denlinger RP (2001) Flow of variably fluidized granular masses across three-dimensional terrain: 1. coulomb mixture theory. J Geophys Res: Solid Earth 106 (B1)537–552
4. Laigle D, Coussot P (1997) Numerical modeling of mudflows. J Hydraul Eng 123(7):617–623
5. O'Brien J, Julien P, Fullerton W (1993) Two-dimensional water flow and mudflow simulation. J Hydraul Eng 119(2):244–261
6. Savage S, Hutter K (1989) The motion of a finite mass of granular material down a rough incline. J Fluid Mech 199:39–54
7. Rickenmann D (1999) Empirical relationships for debris flows. Nat Hazards 19:47–77
8. Wang Y, Hutter K, Pudasaini SP (2004) The savage-hutter theory: A system of partial differential equations for avalanche flows of snow, debris, and mud. ZAMM-J Appl Math Mech/Zeitschrift für Angewandte Mathematik und Mechanik: Appl Math Mech 84(8):507–527

9. Graf C, Christen M, McArdell B, Bartelt P (2019) An overview of a decade of applied debris-flow runout modeling in switzerland: challenges and recommendations. 685–692
10. Rickenmann D, Laigle D, McArdell B, Hübl J (2006) Comparison of 2d debris-flow simulation models with field events. Comput Geosci 10(2):241–264
11. McArdell BW, Sartori M (2020) The illgraben torrent system. In Landscapes and Landforms of Switzerland. Springer, pp. 367–378
12. Iverson RM (1997) The physics of debris flows. Rev Geophys 35(3):245–296
13. McArdell B, Bartelt P, Kowalski J (2007) Field observations of basal forces and fluid pore pressure in a debris flow. Geophys Res Lett 34:L07406
14. Schraml K, Thomschitz B, McArdell BW, Graf C, Kaitna R (2015) Modeling debris-flow runout patterns on two alpine fans with different dynamic simulation models. Natural Hazards and Earth System Science (NHESS) 15(7):1483–1492
15. Iverson RM, George DLA (2014) depth-averaged debris-flow model that includes the effects of evolving dilatancy. i. physical basis. Proc R Soc A: Mathematical, Physical and Engineering Sciences 470(2170):20130819
16. Kowalski J (2008) Two-phase modeling of debris flows. ETH Zurich
17. Kowalski J, McElwaine JN (2013) Shallow two-component gravity-driven flows with vertical variation. J Fluid Mech 714:434–462
18. Pitman EB, Le L (2005) A two-fluid model for avalanche and debris flows. Philosophical Transactions of the Royal Society A: Mathematical, Physical and Engineering Sciences 363(1832):1573–1601
19. Pudasaini SP (2012) A general two-phase debris flow model. J Geophys Res Earth Surf 117:F3
20. Hutter K, Shneider L (2010) Important aspects in the formulation of solid–fluid debris-flow models. part i. thermodynamic implications. Contin Mech Thermodyn 22(5):363–390
21. Badoux A, Graf C, Rhyner J, Kuntner R, McArdell BW (2009) A debris-flow alarm system for the alpine illgraben catchment: design and performance. Nat Hazards 49(3):517–539
22. Schlunegger F, Badoux A, McArdell BW, Wendeler C, Schnydrig D, Rieke-Zapp D, Molnar P (2009) Limits of sediment transfer in an alpine debris-flow catchment, illgraben, switzerland. Quatern Sci Rev 28(11–12):1097–1105
23. Greco M, Iervolino M, Leopardi A, Vacca A (2012) A two-phase model for fast geomorphic shallow flows. Int J Sedim Res 27(4):409–425
24. Johnson C, Kokelaar B, Iverson RM, Logan M, LaHusen R, Gray J (2012) Grain-size segregation and levee formation in geophysical mass flows. J Geophys Res Earth Surf 117:F1
25. Takahashi T (1981) Debris flow. Annu Rev Fluid Mech 13(1):57–77
26. Buser O, Bartelt P (2009) Production and decay of random kinetic energy in granular snow avalanches. J Glaciol 55(189):3–12
27. Visser J. Van (1989) Van der waals and other cohesive forces affecting powder fluidization. Powder Technol 58(1):1–10
28. Bartelt P, Buser O (2016) The relation between dilatancy, effective stress and dispersive pressure in granular avalanches. Acta Geotech 11(3):549–557
29. Bartelt P, Buser O, Vera Valero C, Bühler Y (2016) Configurational energy and the formation of mixed flowing/powder snow and ice avalanches. Ann Glaciol 57(71):179–188
30. Bartelt P, McArdell B, Graf C, Christen M, Buser O (2016) Dispersive pressure, boundary jerk and configurational changes in debris flows. Int J Eros Cont Eng 9(1):1–6
31. Reynolds O (1885) Lvii. on the dilatancy of media composed of rigid particles in contact. with experimental illustrations. The London, Edinburgh, and Dublin Philosophical Magazine and J Sci 20(127):469–481
32. Mandli K (2011) T.Finite volume methods for the multilayer shallow water equations with applications to storm surges. PhD thesis
33. Savary É, Zech Y (2007) Boundary conditions in a two-layer geomorphological model. application to a. J Hydraul Res 45(3):316–332
34. Salm B (1993) Flow, flow transition and runout distances of flowing avalanches. Ann Glaciol 18:221–226
35. Armanini A, Fraccarollo L, Rosatti G (2009) Two-dimensional simulation of debris flows in erodible channels. Computers & Geosciences 35(5):993–1006
36. Castro MJ, Garcıa-Rodrıguez JA, González-Vida JM, Macıas J, Parés C, Vázquez-Cendón ME (2004) Numerical simulation of two-layer shallow water flows through channels with irregular geometry. J Comput Phys 195(1):202–235
37. Christen M, Kowalski J, Bartelt P (2010) Ramms: Numerical simulation of dense snow avalanches in three-dimensional terrain. Cold Reg Sci Technol 63(1–2):1–14
38. Rong G, Wang X, Xu H, Xiao B (2020) Multifactor regression analysis for predicting embankment dam breaching parameters. J Hydraul Eng 146(2):04019051

G. Meyrat (✉) · **K. Ivanova**
WSL Institute for Climate Change, Extremes and Natural Hazards in Alpine Regions CERC, Davos, Switzerland
Email: guillaume.meyrat@slf.ch

B. McArdell
WSL Institute for Forest, Snow and Landscape Research, Birmensdorf, Switzerland

C. Müller
Department of Mechanical and Process Engineering, ETH Zürich, Zürich, Switzerland

P. Bartelt
WSL Institute for Snow and Avalanche Research SLF, Davos, Switzerland